Biomed Microdevices (2013) 15:941–948
DOI 10.1007/s10544-013-9784-6

Enrichment of prostate cancer cells from blood cells with a hybrid dielectrophoresis and immunocapture microfluidic system

Chao Huang · He Liu · Neil H. Bander · Brian J. Kirby

Published online: 27 June 2013

Abstract The isolation of circulating tumor cells (CTCs) from cancer patient blood is a technical challenge that is often addressed by microfluidic approaches. Two of the most prominent techniques for rare cancer cell separation, immunocapture and dielectrophoresis (DEP), are currently limited by a performance tradeoff between high efficiency and high purity. The development of a platform capable of these two performance criteria can potentially be facilitated by incorporating both DEP *and* immunocapture. We present a hybrid DEP-immunocapture system to characterize how DEP controls the shear-dependent capture of a prostate cancer cell line, LNCaP, and the nonspecific adhesion of peripheral blood mononuclear cells (PBMCs). Characterization of cell adhesion with and without DEP effects was performed in a Hele-Shaw flow cell that was functionalized with the prostate-specific monoclonal antibody, J591. In this model system designed to make nonspecific PBMC adhesion readily apparent, we demonstrate LNCaP enrichment from PBMCs by precisely tuning the applied AC electric field frequency to enhance immunocapture of LNCaPs and reduce nonspecific adhesion of PBMCs with positive and negative DEP, respectively. Our work shows that DEP and immunocapture techniques can work synergistically to improve cancer cell capture performance, and it informs the design of future hybrid DEP-immunocapture systems with improved CTC capture performance to facilitate research on cancer metastasis and drug therapies.

Keywords Prostate cancer · Dielectrophoresis · Immunocapture · Circulating tumor cell · Enrichment · Microfluidic

C. Huang
Department of Biomedical Engineering, Cornell University, Ithaca, NY 14853, USA

H. Liu · N. H. Bander
Department of Urology, Weill Medical College of Cornell University, New York, NY 10065, USA

B. J. Kirby (✉)
Sibley School of Mechanical and Aerospace Engineering, Cornell University, Ithaca, NY 14853, USA
e-mail: kirby@cornell.edu

B. J. Kirby
Division of Hematology and Medical Oncology, Department of Medicine, Weill Medical College of Cornell University, New York, NY 10065, USA

1 Introduction

The isolation of circulating tumor cells (CTCs)—cells that have been shed into the circulatory system from a tumor source—enables genetic and pharmacological evaluation of cancer (Leversha et al. 2009; Stott et al. 2010b; Kirby et al. 2012; Rhim et al. 2012; Yu et al. 2012). Oftentimes, such studies require extremely pure samples of captured CTCs; this necessity presents a technical challenge, as CTCs are extremely rare—as few as one cell per 10^8–10^9 blood cells, depending on the definition of CTCs (Racila et al. 1998; Krivacic et al. 2004). Microfluidic immunocapture devices have been used successfully to capture CTCs from cancer patient blood with high efficiency, although capture purity can still potentially be improved by reducing the nonspecific adhesion of leukocytes (Nagrath et al. 2007; Gleghorn et al. 2010; Stott et al. 2010a; Wang et al. 2011; Kirby et al. 2012). Dielectrophoresis (DEP) is an alternative technique to using surface immunological interactions for cell capture (Voldman 2006; Hawkins et al. 2009); previous work on DEP separation of cancer cells is covered in other reviews (Pratt et al. 2011; Hyun and Jung 2013). Examples of recent

DEP techniques for isolating rare cancer cells include flow-field fractionation (DEP-FFF) (Gupta et al. 2012; Shim et al. 2013b), contactless DEP (Henslee et al. 2011; Salmanzadeh et al. 2012), and streamline separations by use of unique geometric features (Alshareef et al. 2013; Jen et al. 2012). Despite the advantage of not requiring biochemical labeling to achieve separation, the use of DEP techniques for CTC capture is currently limited by low throughput and efficiency owing to the rarity of CTCs in whole blood, and also by restrictions of electrode design and DEP physics (Pratt et al. 2011). Given that DEP and immunocapture techniques both have unique advantages and limitations, a combination of both techniques (e.g., applying DEP effects near immunocapture surfaces where electric fields are strongest and antibody interactions occur) can potentially lead to a platform capable of high capture efficiency *and* purity to facilitate subsequent biological analyses of captured CTCs.

A majority of DEP separation methods rely on differences in the electrical properties of cancer cells and blood cells, which lead to distinct DEP responses as a function of applied AC electric field frequency. In frequency ranges in which positive DEP (pDEP) occurs, cells are attracted to stronger electric field regions; conversely, when negative DEP (nDEP) occurs, cells are repelled from stronger field regions. Because cancer cells and blood cells transition from nDEP to pDEP at a different frequency (i.e., they have different "crossover" frequencies), DEP separation is typically achieved by selecting a frequency range in which cancer cells undergo pDEP and blood cells undergo nDEP to actuate the cells in different directions (Gascoyne et al. 2009; Henslee et al. 2011; Gupta et al. 2012). Researchers have characterized the DEP response of erythrocytes and peripheral blood mononuclear cells (PBMCs), as well as a wide variety of cultured cancer cells, as a function of frequency (Sano et al. 2011b; Huang et al. 2013; Han et al. 2013; Salmanzadeh et al. 2013). Of note, Shim et al. characterized the DEP crossover frequency of each NCI-60 cancer cell line and showed that all cancer types except leukemia have crossover frequencies in a range that is distinct from those of blood cells (Shim et al. 2013a). These results suggest that for solid tumors, the applied frequency can potentially be tuned to guide CTCs toward immunocapture surfaces with pDEP while repelling leukocytes and other blood contaminants with nDEP, leading to an improved capture purity (Pratt et al. 2011; Huang et al. 2013).

We have previously shown that the immunocapture of LNCaPs, a prostate cancer cell line, can be augmented by DEP; our work was the first to demonstrate DEP as a complement to existing cancer cell immunocapture techniques for improved cell capture (Huang et al. 2013). In the current study, we characterized the adhesion of LNCaPs and PBMCs to immunocapture surfaces with and without DEP effects as a function of the local shear stress experienced by cells. This characterization was performed in a Hele-Shaw flow cell that was functionalized with the monoclonal antibody, J591, which is highly specific to the prostate-specific membrane antigen (PSMA) expressed on LNCaPs (Liu et al. 1997; Huang et al. 2013). We enriched LNCaPs from PBMCs with DEP by tuning the applied frequency to differentially separate the two populations; this result demonstrates that DEP and immunocapture techniques can work synergistically to improve cancer cell capture performance. Our work informs the design of future hybrid DEP-immunocapture devices with improved CTC capture purity, which has the potential to facilitate subsequent genetic and post-translational modification studies for the development of personalized therapies for cancer patients based on analyses of their own CTCs (Kirby et al. 2012; Diamond et al. 2012).

2 Materials and methods

2.1 Device design, fabrication, and antibody functionalization

A Hele-Shaw flow cell was designed to facilitate the characterization of DEP-guided immunocapture as a function of shear stresses corresponding to those experienced by cells in immunocapture devices (Murthy et al. 2004; Santana et al. 2012; Huang et al. 2013). Figure 1 depicts the Hele-Shaw flow cell with branching inlet channels to distribute entering cells uniformly across the main channel width. The sidewalls are sections of rectangular hyperbolas that replicate the far field of a stagnation flow impinging on the coordinate origin of the hyperbolas; this geometry produces a monotonically decreasing shear stress distribution along the length of the device's central axis (Usami et al. 1993). The device geometry also generates diverging streamlines, which change the local incident cell density; these nonuniformities are known, and are corrected for when the data is analyzed. Interdigitated electrodes were fabricated on only one side of the device's central axis to directly compare cell adhesion with and without DEP effects (Huang et al. 2013).

The Hele-Shaw flow cell was fabricated with standard photolithography and thin-film deposition techniques; details of these processes are described in our previous work (Huang et al. 2013). To summarize, the channel was defined in polydimethylsiloxane (PDMS) by use of an SU-8 master, and bonded to glass that was patterned with interdigitated electrodes. The electrodes were fabricated by depositing a 250-nm layer of gold between 20-nm layers of chromium, cleaned with Cyantek Nano-Strip, and connected externally to wires with silver conductive epoxy. Inlet and outlet holes were created with a biopsy punch and

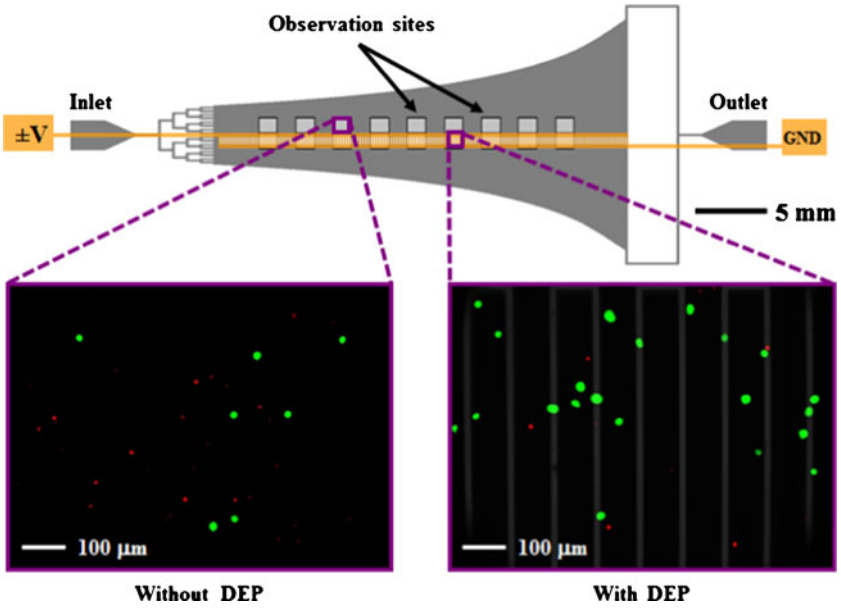

Fig. 1 Schematic of the Hele-Shaw flow cell and its interdigitated electrodes with lead connections to an applied voltage (±V) and ground (GND). Inset images show fluorescently labeled LNCaPs (*green*) and PBMCs (*red*) adhered to the antibody-functionalized surface with and without DEP effects. These example images show that at an applied AC electric field frequency of 350 kHz, more LNCaPs and fewer PBMCs are captured with DEP as compared to without DEP. Captured cells in each pair of 1-mm^2 observation windows were enumerated and compared at a series of observation sites corresponding to a range of shear stresses. Details of the device geometry and shear stress distribution are described in our previous work (Huang et al. 2013)

connected to external tubing. The fully constructed Hele-Shaw flow cell was then functionalized with the humanized monoclonal biotinylated antibody, J591 (manufactured by Lonza Biologics plc for BZL Biologics Inc.), which we have previously characterized (Liu et al. 1997; Santana et al. 2012; Huang et al. 2013) and used for immunocapture of prostate CTCs (Gleghorn et al. 2010; Kirby et al. 2012). The antibody was immobilized on the device's glass surface at an incubating solution concentration of 5 μg/mL by use of MPTMS–GMBS–NeutrAvidin–biotin chemistry following previously reported protocols (Gleghorn et al. 2010; Santana et al. 2012).

2.2 Cell culture and preparation

LNCaPs, an immortalized, PSMA-expressing prostate cancer cell line, were purchased from the American Type Culture Collection, and cultured in Corning cellgro® RPMI 1640 supplemented with 10 % fetal bovine serum and 1 % penicillin-streptomycin in CellBIND T75 culture flasks at 37 °C in a 5 % CO_2 humidified environment. To prepare for experiments, LNCaPs were trypsinized from their flask, resuspended in phosphate-buffered saline (PBS), labeled with CellTracker™ Green CMFDA (Invitrogen), and incubated for 30 min.

PBMCs were isolated from the blood of healthy donors with approval from the Institutional Review Board for Human Participants. Whole blood was collected in BD Vacutainer® CPT™ Cell Preparation Tubes with Sodium Heparin^N, and centrifuged at 1700×g for 15 min. PBMCs above the polyester gel were then collected in a separate conical tube, washed with PBS by centrifuging at 300×g for 15 min twice, resuspended in PBS, labeled with CellTracker™ Orange CMRA (Invitrogen), and incubated for 30 min.

After incubation with their respective fluorescent probes, LNCaPs and PBMCs were washed twice and resuspended in PBS diluted 20 times by volume in an isotonic sugar in deionized (DI) H_2O solution consisting of 9.5 % sucrose and 0.3 % dextrose with conductivity 0.07 S/m. This sugar solution is similar to that used by other researchers studying DEP separation of cancer cells (Gupta et al. 2012; Shim et al. 2013b; Huang et al. 2013), and was chosen because of the distinct DEP response that cancer cells and blood cells exhibit at the given conductivity (see next section). The final cell densities were 5×10^5 LNCaPs per mL and 2×10^6 PBMCs per mL; the two populations were mixed together before injection into the Hele-Shaw flow cell.

2.3 DEP characterization of cells

The sign and magnitude of the time-averaged DEP force, $\langle \mathbf{F}_{DEP} \rangle$, on a spherical particle in an infinite domain with

homogeneous and isotropic complex permittivities is determined by the real part of the Clausius-Mossotti factor, $\Re\left(\tilde{f}_{\mathrm{CM}}\right)$:

$$\langle \mathbf{F}_{\mathrm{DEP}} \rangle = \pi \varepsilon_{\mathrm{m}} a^3 \Re\left(\tilde{f}_{\mathrm{CM}}\right) \nabla(\mathbf{E}_0 \cdot \mathbf{E}_0) \quad (1)$$

$$\tilde{f}_{\mathrm{CM}} = \frac{\tilde{\varepsilon}_{\mathrm{p}} - \tilde{\varepsilon}_{\mathrm{m}}}{\tilde{\varepsilon}_{\mathrm{p}} + 2\tilde{\varepsilon}_{\mathrm{m}}} \quad (2)$$

where a is the particle radius, $\mathbf{E} = \mathbf{E}_0 \cos(\omega t)$ is the externally applied AC electric field, $\boldsymbol{\omega}$ is the angular frequency of the electric field, $\tilde{\boldsymbol{\varepsilon}} = \boldsymbol{\varepsilon} - \mathbf{i}\boldsymbol{\sigma}/\boldsymbol{\omega}$ is the complex permittivity, $\mathrm{i} = (-1)^{1/2}$, $\boldsymbol{\varepsilon}$ is the electrical permittivity, σ is the electrical conductivity, and the subscripts p and m denote the particle and the medium, respectively (Morgan and Green 2002; Kirby 2010). The frequency at which $\Re\left(\tilde{f}_{\mathrm{CM}}\right) = 0$, i.e., when the particle transitions from nDEP to pDEP, or vice versa, is termed the crossover frequency. Although the cells under study are neither spherical, homogeneous, nor isotropic, this analysis can still be used to a good approximation because effective particle properties can be defined, facilitated by the mathematical properties of the spherical harmonic solutions used in eigenfunction expansion approximations for the DEP force. In this case, $\tilde{\boldsymbol{\varepsilon}}_{\mathrm{p}}$ becomes an extrinsic particle property rather than an intrinsic material property (Hawkins et al. 2009; Kirby 2010).

To determine the crossover frequency range of LNCaPs and PBMCs, the two populations were manually flowed through the Hele-Shaw flow cell and their DEP responses were observed above the interdigitated electrodes region on a Nikon LV100 upright microscope. The electrodes were energized by an Agilent 33200A function generator at 6 volts peak-to-peak (V_{pp}) and frequencies ranging from 100 kHz to 1 MHz. At each applied frequency, we recorded whether each cell population was attracted to or repelled from the electrodes by pDEP and nDEP, respectively, and we determined the frequency range in which the cells were unaffected or affected nonuniformly by the applied electric field (i.e., crossover frequency). After determining each cell population's crossover frequency, we predicted the magnitude of its DEP response as a function of frequency by modeling the cell as a single-shelled dielectric sphere (Morgan and Green 2002; Kirby 2010). The effective permittivity of the particle, $\tilde{\boldsymbol{\varepsilon}}_{\mathrm{p}}$, in Eq. 2, was replaced by an effective permittivity of the cell, $\tilde{\boldsymbol{\varepsilon}}_{\mathrm{cell}}$, that describes its electrical properties in terms of a specific membrane capacitance, C_{membrane}, and the cytoplasmic permittivity and conductivity (Kirby 2010; Huang et al. 2013):

$$\tilde{\boldsymbol{\varepsilon}}_{\mathrm{cell}} = \frac{C_{\mathrm{membrane}}\, a\, \tilde{\boldsymbol{\varepsilon}}_{\mathrm{cytoplasm}}}{C_{\mathrm{membrane}}\, a + \tilde{\boldsymbol{\varepsilon}}_{\mathrm{cytoplasm}}} \quad (3)$$

Interactions between the cell and the electric field occur primarily at the cell membrane, although the physical and electrical properties of the membrane are often difficult to infer from experimental measurements (Voldman 2006; Kirby 2010). Thus, it is common to use the single-shelled dielectric model and extrapolate a specific membrane capacitance to describe the extrinsic properties of the cell (Becker et al. 1995; Gascoyne et al. 2009; Sano et al. 2011b). Figure 2 shows the predicted DEP response of LNCaPs and PBMCs as a function of frequency using this shell model. Under our experimental conditions, varying the cytoplasmic permittivity and conductivity did not significantly change the magnitude of $\Re\left(\tilde{f}_{\mathrm{CM}}\right)$, and thus their values were fixed to $50\boldsymbol{\varepsilon}_0$ ($\boldsymbol{\varepsilon}_0 = 8.85 \times 10^{-12}$ F/m) and 1 S/m, respectively, which are within the range of previously reported values for cancer cells and blood cells (Becker et al. 1995; Sano et al. 2011b; Han et al. 2013; Shim et al. 2013a). The average cell radius was measured to be approximately 10 μm for LNCaPs and 5 μm for PBMCs. Through detailed characterization of LNCaPs' DEP response (Huang et al. 2013) and analysis of measured and predicted crossover frequencies, we selected 250 kHz and 350 kHz as the frequencies to apply in characterizing pDEP and nDEP effects on cell adhesion as a function of shear stress. As shown in Fig. 2, both LNCaPs and PBMCs exhibit a nDEP response at 250 kHz; however, at 350 kHz, LNCaPs exhibit a pDEP response whereas PBMCs exhibit a nDEP response.

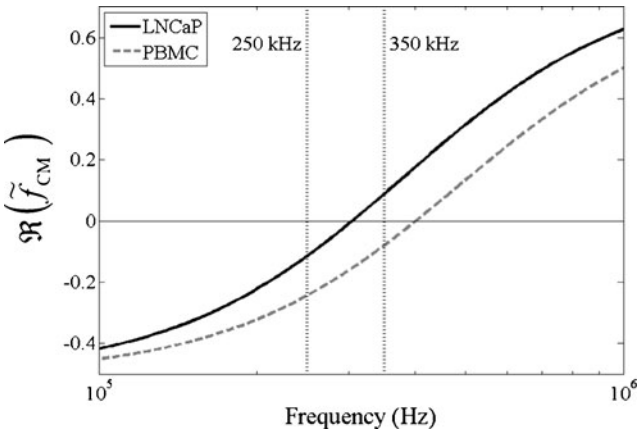

Fig. 2 Predicted DEP response, as described by $\Re\left(\tilde{f}_{\mathrm{CM}}\right)$, of LNCaPs (*solid line*) and PBMCs (*dashed line*) as a function of applied electric field frequency. Cells were modeled as single-shelled dielectric spheres, described by Eqs. 2 and 3. In a diluted PBS suspending medium with $\sigma_{\mathrm{m}} = 0.07$ S/m, the crossover frequency was experimentally determined to be approximately 300 kHz for LNCaPs and 400 kHz for PBMCs. These empirical measurements, combined with Eq. 3, corresponded to specific membrane capacitance values of $C_{\mathrm{membrane}} = 5$ mF/m^2 and $C_{\mathrm{membrane}} = 7.5$ mF/m^2 for LNCaPs and PBMCs, respectively, in the dielectric shell model. At 250 kHz, both cell populations exhibit a nDEP response; at 350 kHz, however, LNCaPs exhibit a pDEP response whereas PBMCs still exhibit a nDEP response. Comparisons of the two frequencies' effects on DEP-guided immunocapture are shown in Figs. 3a and 3b

2.4 DEP-guided enrichment of LNCaPs from PBMCs

To characterize cell adhesion of LNCaPs and PBMCs as a function of shear stress, a mixture of the two cell populations was flowed through the Hele-Shaw flow cell and captured cells were enumerated along the length of the device. The cell mixture was drawn into a BD plastic syringe and flowed through the device at 0.2 mL/hr with a Chemyx Fusion 400 syringe pump for 5 minutes. The interdigitated electrodes were energized by an Agilent 33200A function generator at 6 V_{pp} and two different frequencies: 250 kHz and 350 kHz, with six experimental replicates each. After each capture experiment, PBS was flowed through the device at 0.2 mL/hr for 10 minutes to wash away any non-adherent cells. Fluorescent images of captured LNCaPs and PBMCs were taken at a 20x magnification with FITC and Texas Red® / Cy3.5™ Chroma filter cubes, respectively, at a series of observation sites along the length of the device, as shown in Fig. 1. Reported captured cell densities correspond to the number of captured cells multiplied by a correction factor (to normalize for streamline divergence in the device) in an observation window with a shear stress at the immunocapture surface in the center of the imaged area (Huang et al. 2013). Captured cell densities of both LNCaPs and PBMCs were compared between either side of the Hele-Shaw flow cell's central axis to characterize the effect of DEP on cell adhesion at each shear stress value.

3 Results and discussion

The DEP-guided immunocapture performance of LNCaPs and nonspecific adhesion of PBMCs to antibody-functionalized surfaces was characterized as a function of shear stresses corresponding to those experienced by cells in immunocapture devices (Santana et al. 2012; Kirby et al. 2012; Huang et al. 2013). A mixture of LNCaPs and PBMCs was flowed through the Hele-Shaw flow cell and captured cells were enumerated under three experimental conditions: no DEP, 250 kHz, and 350 kHz. Figures 3a and b show the captured cell densities as a function of shear stress for LNCaPs and PBMCs, respectively, under these experimental conditions. Of note, the solution used for these experiments was purposely free of factors known to suppress nonspecific adhesion, which include Pluronic® surfactants (Hawkins et al. 2007, 2011, Huang et al. 2013) and bovine serum albumin (Gleghorn et al. 2010; Santana et al. 2012). This omission maximizes nonspecific adhesion, which would be problematic for rare cell capture but is required in this study to make PBMC capture measurable at cell counts comparable to LNCaP cell counts. In rare cell capture applications, surfactants or blocking proteins are used, and the PBMC capture rate is typically much lower, but the ratio of PBMCs to target cells is still high enough that PBMCs are the primary contaminant (Pratt et al. 2011). Our experiments inform the *relative* capture of PBMCs but, because of the solutions and cell densities used, purposely study a condition that overestimates the absolute magnitude of PBMC capture.

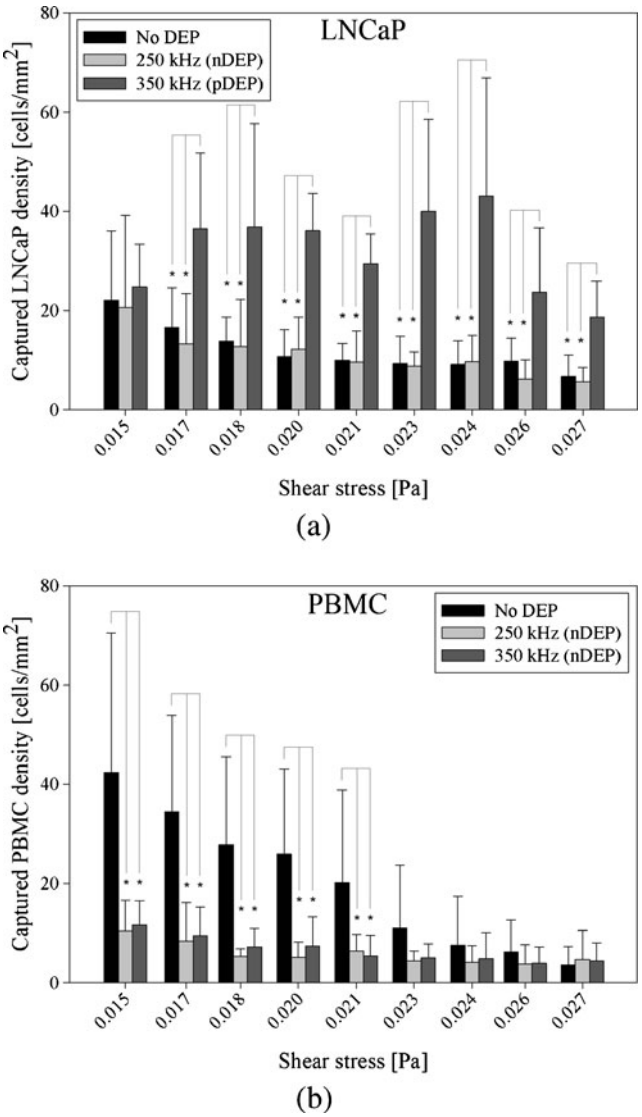

Fig. 3 Captured cell density of LNCaPs, Figs. 3a, and PBMCs, 3b, as a function of shear stress under experimental conditions of no DEP (*black bars*; $n = 12$), 6 V_{pp} at 250 kHz (*light gray bars*; $n = 6$), and 6 V_{pp} at 350 kHz (*dark gray bars*; $n = 6$). *Bars* represent the mean captured cell density normalized for streamline divergence in the Hele-Shaw flow cell, and *error bars* represent standard deviation. A Kruskal-Wallis ANOVA test was used to compare between the experimental conditions. For the LNCaP data, *asterisks* (*) indicate significance of differences ($P < 0.05$) between the 350 kHz and no-DEP conditions and between the 350 kHz and 250 kHz conditions. For the PBMC data, *asterisks* indicate significance of differences ($P < 0.05$) between the no-DEP and 250 kHz conditions and between the no-DEP and 350 kHz conditions

At 250 kHz, LNCaPs exhibit a weak nDEP response whereas PBMCs exhibit a stronger nDEP response (as predicted in Fig. 2); thus, it is expected that as the magnitude of the nDEP response increases, cells flowing past regions with energized interdigitated electrodes (as depicted in Fig. 1) will be repelled further from the antibody-functionalized surface. Figures 3a and b show that under this DEP condition, LNCaP capture via immunological interactions with the antibody was not significantly affected, while significantly fewer PBMCs were captured by nonspecific adhesion as compared to conditions without DEP at a majority of reported shear stresses. The ratio of captured cell densities with DEP to without DEP averaged across all shear stresses was calculated to be 0.91 for LNCaPs and 0.45 for PBMCs under the 250 kHz condition, as shown in Fig. 4. The ratio for LNCaPs is marginally less than 1, indicating that the cells exhibited a minimal nDEP response that resulted in negligibly fewer cells being captured as compared to without DEP. In contrast, the ratio for PBMCs is much smaller than 1, indicating that the cells exhibited a strong nDEP response that resulted in significantly fewer cells being captured as compared to without DEP. The conclusions drawn from these comparisons of captured cell densities are supported by tests of statistical significance (Fig. 3).

At 350 kHz, LNCaPs exhibit a pDEP response whereas PBMCs exhibit a nDEP response (as predicted in Fig. 2); under this condition, it is expected that LNCaPs will

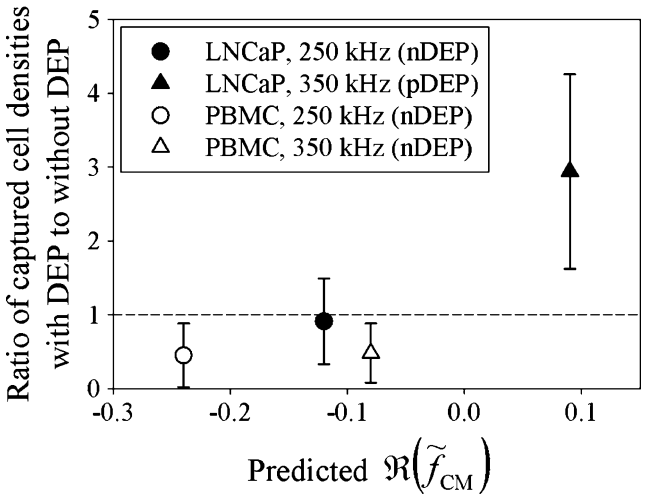

Fig. 4 Ratios of captured LNCaP and PBMC densities with DEP to without DEP effects averaged across all reported shear stresses shown in Fig. 3. *Error bars* represent standard error of the mean of ratios. Predicted $\Re\left(\tilde{f}_{CM}\right)$ values were taken from the single-shelled dielectric model plotted in Fig. 2. At 250 kHz, LNCaPs and PBMCs both exhibit a nDEP response, resulting in a calculated ratio less than 1 (i.e., fewer cells were captured with DEP as compared to without DEP). In contrast, at 350 kHz, LNCaPs exhibit a pDEP response that resulted in a ratio much larger than 1 (i.e., more LNCaPs were captured with DEP as compared to without DEP), whereas PBMCs still exhibit a nDEP response that resulted in a ratio less than 1

be attracted to energized electrodes on the antibody-functionalized surface and that PBMCs will be repelled. Figures 3a and b show that at a majority of shear stresses, significantly more LNCaPs and fewer PBMCs were captured with DEP as compared to conditions without DEP. The ratio of captured cell densities with DEP to without DEP averaged across all reported shear stresses was calculated to be 2.94 for LNCaPs and 0.48 for PBMCs under the 350 kHz condition, as shown in Fig. 4. The ratio for LNCaPs is much larger than 1, indicating that the cells exhibited a strong pDEP response that resulted in significantly more cells being captured as compared to without DEP. In contrast, the ratio for PBMCs remains smaller than 1, indicating that the cells continued to exhibit a nDEP response that resulted in significantly fewer cells being captured as compared to without DEP. Once again, the conclusions drawn from these comparisons of captured cell densities are supported by tests of statistical significance (Fig. 3). In summary, DEP-guided immunocapture of LNCaPs was diminished at 250 kHz and enhanced at 350 kHz, whereas the nonspecific adhesion of PBMCs with DEP was reduced at both 250 kHz and 350 kHz. Therefore, we have shown that by precisely selecting an appropriate frequency, LNCaPs can be enriched from PBMCs with DEP to improve immunocapture performance. Although the ratios presented here do not in themselves justify rare cell capture or enrichment, the device geometry and experimental conditions were chosen to purposely augment nonspecific PBMC adhesion; implementation of DEP conditions in a typical rare cell immunocapture device is expected to lead to significant improvement (Pratt et al. 2011; Gleghorn et al. 2010).

Cell adhesion was not only affected by the addition of DEP, but also by the shear stress experienced by cells in the Hele-Shaw flow cell. Without DEP, captured cell densities generally decreased with increasing shear stress. When a nDEP force was applied to PBMCs, nonspecific adhesion was lower at high shear stresses, resulting in statistically insignificant differences between the no-DEP and nDEP conditions (Fig. 3b). However, when a pDEP force was applied to LNCaPs, captured cell densities were consistently and statistically greater than the no-DEP condition across the entire shear stress range (Fig. 3a). This result suggests that in designing future hybrid DEP-immunocapture devices for CTC capture (Pratt et al. 2011; Smith et al. 2012; Huang et al. 2013), shear stress (as controlled by flow rate) is an adjustable parameter that can be optimized. For example, flow rate can be increased to minimize interactions between leukocytes and immunocapture surfaces, and the addition of DEP can further reduce nonspecific leukocyte adhesion and promote interactions between CTCs and immunocapture surfaces.

DEP is an advantageous technique because, in many cases, the applied frequency can be tuned to separate cell

populations based on differences in their electrical properties. We have previously characterized the DEP response of LNCaPs (Huang et al. 2013) and, in this study, have shown that prostate cancer cells exhibit a distinct response as compared to PBMCs. Furthermore, in this study, we used a diluted PBS media that is 5–50 times less dilute and 2–7 times more conductive than media used in previous DEP studies (Becker et al. 1995; Gascoyne et al. 2009; Henslee et al. 2011; Sano et al. 2011a; Gupta et al. 2012; Alshareef et al. 2013). We used PBS as a model for whole blood and expect to demonstrate similar cancer cell capture and enrichment results in minimally diluted blood, which can potentially result in improved throughput and efficiency as compared to current DEP devices. Recently, Shim et al. introduced a media-deionizing region to the previously reported DEP-FFF device (Gascoyne et al. 2009; Gupta et al. 2012); depleting ions in the sample decreases the medium conductivity to a level at which differential DEP separation of cancer and blood cells is possible, and serves an alternative technique to diluting whole blood (Shim et al. 2013b; Shim et al. 2013a).

Our characterization data of DEP-guided immunocapture of cancer cells as a function of shear stress can also be incorporated into computational fluid dynamics simulations of cancer cell and blood cell trajectories in a 3D immunocapture device to better predict differential capture performance (Gleghorn et al. 2010; Kirby et al. 2012; Smith et al. 2012). These simulations will inform the design of future hybrid DEP-immunocapture systems that have the potential to improve CTC capture purity while retaining the capture efficiency of previous immunocapture devices (Nagrath et al. 2007; Gleghorn et al. 2010; Stott et al. 2010a; Wang et al. 2011). The capability of producing a highly pure sample will in turn facilitate subsequent biological studies on captured CTCs, cancer metastasis, and drug therapies (Leversha et al. 2009; Stott et al. 2010b; Kirby et al. 2012; Yu et al. 2012).

4 Conclusions

This work characterizes the DEP-enhanced immunocapture of LNCaPs and nonspecific adhesion of PBMCs to antibody-functionalized surfaces as a function of shear stress. In a model system designed to make nonspecific PBMC adhesion readily apparent, we showed that LNCaPs can be enriched from PBMCs by precisely tuning the frequency of the applied electric field to attract cancer cells to and repel leukocytes from immunocapture surfaces. This result is dependent on local shear stresses experienced by cells, and informs the design (e.g., geometric features) and optimization (e.g., flow rate, applied frequency) of future hybrid DEP-immunocapture devices for rare cell capture. We expect that such a combination will lead to improved capture performance relative to either technique alone, which will facilitate subsequent biological analyses of captured CTCs.

Acknowledgments This work was supported by the Center on the Microenvironment and Metastasis at Cornell (Award Number U54CA-143876) from the National Cancer Institute Physical Sciences Oncology Center (NCI PS-OC). CH was supported by a National Science Foundation (NSF) Graduate Research Fellowship. Device fabrication was performed in part at the Cornell NanoScale Science and Technology Facility (CNF), a member of the National Nanotechnology Infrastructure Network, which is supported by the NSF (Grant ECS-0335765).

References

M. Alshareef, N. Metrakos, E. Juarez Perez, F. Azer, F. Yang, X. Yang, G. Wang, Separation of tumor cells with dielectrophoresis-based microfluidic chip. Biomicrofluidics **7**(1), 011,803 (2013)

F.F. Becker, P.R. Gascoyne, X.B. Wang, Y. Huang, R. Pethig, J. Vykoukal, Separation of human breast cancer cells from blood by differential dielectric affinity. Proc. Natl. Acad. Sci. U.S.A. **92**(3), 860–864 (1995)

E. Diamond, G.Y. Lee, N.H. Akhtar, B.J. Kirby, P. Giannakakou, S.T. Tagawa, D.M. Nanus, Isolation and characterization of circulating tumor cells in prostate cancer. Front. Oncol. **2**, 131 (2012)

P.R.C. Gascoyne, J. Noshari, T.J. Anderson, F.F. Becker, Isolation of rare cells from cell mixtures by dielectrophoresis. Electrophor. **30**(8), 1388–1398 (2009)

J.P. Gleghorn, E.D. Pratt, D. Denning, H. Liu, N.H. Bander, S.T. Tagawa, D.M. Nanus, P.A. Giannakakou, B.J. Kirby, Capture of circulating tumor cells from whole blood of prostate cancer patients using geometrically enhanced differential immunocapture (GEDI) and a prostate-specific antibody. Lab Chip. **10**(1), 27–29 (2010)

V. Gupta, I. Jafferji, M. Garza, V.O. Melnikova, D.K. Hasegawa, R. Pethig, D.W. Davis, ApoStream, a new dielectrophoretic device for antibody independent isolation and recovery of viable cancer cells from blood. Biomicrofluidics **6**(2), 024,133 (2012)

S.I. Han, Y.D. Joo, K.H. Han, An electrorotation technique for measuring the dielectric properties of cells with simultaneous use of negative quadrupolar dielectrophoresis and electrorotation. The Anal. **138**(5), 1529–1537 (2013)

B.G. Hawkins, A.E. Smith, Y.A. Syed, B.J. Kirby, Continuous-flow particle separation by 3D insulative dielectrophoresis using coherently shaped, dc-biased, ac electric fields. Anal. Chem. **79**(19), 7291–7300 (2007)

B.G. Hawkins, J.P. Gleghorn, B.J. Kirby, in *Dielectrophoresis for Particle and Cell Manipulations*, ed. by J.D. Zahn. Methods in Bioengineering: Biomicrofabrication and Biomicrofluidics, chap. 6 (Artech House, Boston, 2009), pp. 133–181

B.G. Hawkins, C. Huang, S. Arasanipalai, B.J. Kirby, Automated dielectrophoretic characterization of Mycobacterium smegmatis. Anal. Chem. **83**(9), 3507–3515 (2011)

E.A. Henslee, M.B. Sano, A.D. Rojas, E.M. Schmelz, R.V. Davalos, Selective concentration of human cancer cells using contactless dielectrophoresis. Electrophoresis **32**(18), 2523–2529 (2011)

C. Huang, S.M. Santana, H. Liu, N.H. Bander, B.G. Hawkins, B.J. Kirby, Characterization of a hybrid dielectrophoresis and immunocapture microfluidic system for cancer cell capture. submitted (2013)

K.A. Hyun, H.I. Jung, Microfluidic devices for the isolation of circulating rare cells: a focus on affinity-based, dielectrophoresis, and hydrophoresis. Electrophoresis. **34**(7), 1028–1041 (2013)

C.P. Jen, H.H. Chang, C.T. Huang, K.H. Chen, A microfabricated module for isolating cervical carcinoma cells from peripheral blood utilizing dielectrophoresis in stepping electric fields. Microsyst. Technol. **18**(11), 1887–1896 (2012)

B.J. Kirby, *Micro- and Nanoscale Fluid Mechanics: Transport in Microfluidic Devices* (Cambridge University Press, New York, 2010)

B.J. Kirby, M. Jodari, M.S. Loftus, G. Gakhar, E.D. Pratt, C. Chanel-Vos, J.P. Gleghorn, S.M. Santana, H. Liu, J.P. Smith, V.N. Navarro, S.T. Tagawa, N.H. Bander, D.M. Nanus, P. Giannakakou, Functional characterization of circulating tumor cells with a prostate-cancer-specific microfluidic device. PLOS ONE. **7**(4), e35,976 (2012)

R.T. Krivacic, A. Ladanyi, D.N. Curry, H.B. Hsieh, P. Kuhn, D.E. Bergsrud, J.F. Kepros, T. Barbera, M.Y. Ho, L.B. Chen, R.A. Lerner, R.H. Bruce, A rare-cell detector for cancer. Proc. Natl. Acad. Sci. U.S.A. **101**(29), 10,501–10,504 (2004)

M.A. Leversha, J. Han, Z. Asgari, D.C. Danila, O. Lin, R. Gonzalez-Espinoza, A. Anand, H. Lilja, G. Heller, M. Fleisher, H.I. Scher, Fluorescence *in situ* hybridization analysis of circulating tumor cells in metastatic prostate cancer. Clin. Cancer Res. **15**(6), 2091–2097 (2009)

H. Liu, P. Moy, S. Kim, Y. Xia, A. Rajasekaran, V. Navarro, B. Knudsen, N.H. Bander, Monoclonal antibodies to the extracellular domain of prostate-specific membrane antigen also react with tumor vascular endothelium. Cancer Res. **57**(17), 3629–3634 (1997)

H. Morgan, N. Green, AC Electrokinetics: Colloids and Nanoparticles (Research Studies Press, Ltd., Baldock, 2002)

S.K. Murthy, A. Sin, R.G. Tompkins, M. Toner, Effect of flow and surface conditions on human lymphocyte isolation using microfluidic chambers. Langmuir. **20**(26), 11,649–11,655 (2004)

S. Nagrath, L.V. Sequist, S. Maheswaran, D.W. Bell, D. Irimia, L. Ulkus, M.R. Smith, E.L. Kwak, S. Digumarthy, A. Muzikansky, P. Ryan, U.J. Balis, R.G. Tompkins, D.A. Haber, M. Toner, Isolation of rare circulating tumour cells in cancer patients by microchip technology. Nature **450**(7173), 1235–1239 (2007)

E.D. Pratt, C. Huang, B.G. Hawkins, J.P. Gleghorn, B.J. Kirby, Rare cell capture in microfluidic devices. Chem. Eng. Sci. **66**(7), 1508–1522 (2011)

E. Racila, D. Euhus, A.J. Weiss, C. Rao, J. McConnell, L.W.M.M. Terstappen, J.W. Uhr, Detection and characterization of carcinoma cells in the blood. Proc. Natl. Acad. Sci. U.S.A. **95**(8), 4589–94 (1998)

A.D. Rhim, E.T. Mirek, N.M. Aiello, A. Maitra, J.M. Bailey, F. McAllister, M. Reichert, G.L. Beatty, A.K. Rustgi, R.H. Vonderheide, S.D. Leach, B.Z. Stanger, EMT and dissemination precede pancreatic tumor formation. Cell **148**(1–2), 349–361 (2012)

A. Salmanzadeh, L. Romero, H. Shafiee, R.C. Gallo-Villanueva, M.A. Stremler, S.D. Cramer, R.V. Davalos, Isolation of prostate tumor initiating cells (TICs) through their dielectrophoretic signature. Lab Chip. **12**(1), 182–189 (2012)

A. Salmanzadeh, M.B. Sano, R.C. Gallo-Villanueva, P.C. Roberts, E.M. Schmelz, R.V. Davalos, Investigating dielectric properties of different stages of syngeneic murine ovarian cancer cells. Biomicrofluidics **7**(1), 011,809 (2013)

M.B. Sano, J.L. Caldwell, R.V. Davalos, Modeling and development of a low frequency contactless dielectrophoresis (cDEP) platform to sort cancer cells from dilute whole blood samples. Biosens. Bioelectron. **30**(1), 13–20 (2011a)

M.B. Sano, E.A. Henslee, E. Schmelz, R.V. Davalos, Contactless dielectrophoretic spectroscopy: examination of the dielectric properties of cells found in blood. Electrophoresis **32**(22), 3164–3171 (2011b)

S.M. Santana, H. Liu, N.H. Bander, J.P. Gleghorn, B.J. Kirby, Immunocapture of prostate cancer cells by use of anti-PSMA antibodies in microdevices. Biomed. Microdevices. **14**(2), 401–407 (2012)

S. Shim, K. Stemke-Hale, J. Noshari, F.F. Becker, P.R.C. Gascoyne, Dielectrophoresis has broad applicability to marker-free isolation of tumor cells from blood by microfluidic systems. Biomicrofluidics **7**(1), 011,808 (2013a)

S. Shim, K. Stemke-Hale, A.M. Tsimberidou, J. Noshari, T.E. Anderson, P.R.C. Gascoyne, Antibody-independent isolation of circulating tumor cells by continuous-flow dielectrophoresis. Biomicrofluidics **7**(1), 011,807 (2013b)

J.P. Smith, A.C. Barbati, S.M. Santana, J.P. Gleghorn, B.J. Kirby, Microfluidic transport in microdevices for rare cell capture. Electrophoresis **33**(21), 3133–3142 (2012)

S.L. Stott, C.H. Hsu, D.I. Tsukrov, M. Yu, D.T. Miyamoto, B.A. Waltman, S.M. Rothenberg, A.M. Shah, M.E. Smas, G.K. Korir, F.P. Floyd, A.J. Gilman, J.B. Lord, D. Winokur, S. Springer, D. Irimia, S. Nagrath, L.V. Sequist, R.J. Lee, K.J. Isselbacher, S. Maheswaran, D.A. Haber, M. Toner, Isolation of circulating tumor cells using a microvortex-generating herringbone-chip. Proc. Natl. Acad. Sci. U.S.A. **107**(43), 18,392–18,397 (2010a)

S.L. Stott, R.J. Lee, S. Nagrath, M. Yu, D.T. Miyamoto, L. Ulkus, E.J. Inserra, M. Ulman, S. Springer, Z. Nakamura, A.L. Moore, D.I. Tsukrov, M.E. Kempner, D.M. Dahl, C.L. Wu, A.J. Iafrate, M.R. Smith, R.G. Tompkins, L.V. Sequist, M. Toner, D.A. Haber, S. Maheswaran, Isolation and characterization of circulating tumor cells from patients with localized and metastatic prostate cancer. Sci. Transl. Med. **2**(25), 25ra23 (2010b)

S. Usami, H.H. Chen, Y. Zhao, S. Chien, R. Skalak, Design and construction of a linear shear stress flow chamber. Ann. Biomed. Eng. **21**(1), 77–83 (1993)

J. Voldman, Electrical forces for microscale cell manipulation. Annu. Rev. Biomed. Eng. **8**, 425–54 (2006)

S. Wang, K. Liu, J. Liu, Z.T.F. Yu, X. Xu, L. Zhao, T. Lee, E.K. Lee, J. Reiss, Y.K. Lee, L.W.K. Chung, J. Huang, M. Rettig, D. Seligson, K.N. Duraiswamy, C.K.F. Shen, H.R. Tseng, Highly efficient capture of circulating tumor cells by using nanostructured silicon substrates with integrated chaotic micromixers. Angew. Chem. Int. Ed. **50**(13), 3084–3088 (2011)

M. Yu, D.T. Ting, S.L. Stott, B.S. Wittner, F. Ozsolak, S. Paul, J.C. Ciciliano, M.E. Smas, D. Winokur, A.J. Gilman, M.J. Ulman, K. Xega, G. Contino, B. Alagesan, B.W. Brannigan, P.M. Milos, D.P. Ryan, L.V. Sequist, N. Bardeesy, S. Ramaswamy, M. Toner, S. Maheswaran, D.A. Haber, RNA sequencing of pancreatic circulating tumour cells implicates WNT signalling in metastasis. Nature. **487**(7408), 510–513 (2012)